IQ Based Direct Sequence Spread Spectrum Spatial Data Focusing implemented over a 6 Ray Urban Canyon Channel Model

Odhiambo Michael[1,2], *Molineaux Guylian*[2,1], *De Doncker Philippe*[2], *and Sarrazin Julien*[1]

[1] *Sorbonne Université, CNRS, Laboratoire de Génie Electrique et Electronique de Paris, 75252, Paris, France, Université Paris-Saclay, CentraleSupélec, CNRS, Laboratoire de GEEPs, 91192, Gif-sur-Yvette, France.,, Email: michael.odhiambo@sorbonne-universite.fr*
[2] *Université Libre de Bruxelles (ULB), OPERA - Wireless Communications Group, CP 165/81 Avenue F. Roosevelt 50 1050 Brussels, Belgium*

Keywords: Spatial Data Focusing, Geocasting, Spread Spectrum Modulation, Beamforming, Antenna Arrays, Multipath Channel models

Abstract:
Spatial Data Focusing is implemented using Direct Sequence Spread Spectrum technique with orthogonal Gold code sequences forming the orthogonal transmit signal basis. IQ resources are used to facilitate additional degree of freedom. With a four element antenna array, it is demonstrated that this scheme attains a beam-width of less than 4°. The robustness of this schemes' performance is assessed using a 6-ray urban canyon multipath micro-cell channel model simulation. (In SDF, the beamwidth is defined as the region within which transmitted signals can be decoded)

Résumé:
La Focalisation Spatiale de Données (FSD) est mise en œuvre en utilisant la technique d'étalement de spectre basée sur des codes orthogonaux dit Gold. Les ressources de I,Q sont utilisées pour faciliter un degré de liberté supplémentaire. En particuliere, il est montre que pour des réseaux d'antennes à quatre éléments, ce schéma atteint une largeur de faisceau inférieure à 4°. La robustesse de cette schéma est évaluée l'aide d'un modèle de canal micro cellulaires à 6 multitrajets (6-Ray Urban Canyon) (En FSD, la faisceau est définie comme la région dans laquelle les signaux transmis peuvent être décodés)

1 Introduction

SDF was proposed as a candidate alternative to classical beamforming in geocasting applications [1–3]. Geocasting being the ability to broadcast data to predefined geographical locations. In this work we seek to demonstrate the robustness of the Complex Code based Direct Sequence Spread Spectrum Spatial Data Focusing over classical Urban micro channels. In this case the 6-Ray Urban Canyon channel. Urban micro (UMi) was chosen due to the fact it is a classic 5G deployment scenario with outdoor to outdoor (O2O) propagation [4]. The subject of geocasting has been extensively researched in the recent past due to its potential implication on futuristic communication applications including the internet of Things (IoT), design of smart cities, specifically in Vehicular Ad-hoc networks (VANets) design, tourist guide applications and wearable gadgets that may require some sort of knowledge about their present environment. One key area that SDF is envisaged to be of great potential is with applications that may aid the physically challenged, say the blind, to easily navigate through their day to day activity, like walking around the city and being kept constantly aware of the state of their location/position. A typical scenario would be at a traffic crossing, here they can get information broadcast about the state of the traffic directly to their connected devices. The unifying specification for all geocasting applications will be accurate **location selectivity** in addition to the need for increased data capacity and speed, in essence, the key promises of the 5G technology. 5G technologies will largely rely on MIMO, beamforming, and other candidate alternatives to beamforming like the proposed Spatial Data Focusing.

In classical scenarios, geocasting is implemented using beam-forming which is an energy focusing technique as opposed to the proposed SDF which seeks to focus the transmitted data. The advent of 5G has reinvigorated work on beamforming in the recent past, albeit, research on beamforming (BF) and phased arrays has been ongoing over decades now [5–10]. The design of beamformers classically involve the use of phase shifters at RF frequencies [7]. This design approach faces several challenges including hardware design complexity and the fact that implementation cost increases with an increase in array aperture which is a requirement to achieve narrower beams. In addition, the fact that phase shifters are inherently low bandwidth equipment will limit this approach on grounds of attainable bandwidth. However this latter challenge can be counteracted by employing Local

Oscillator (LO) phase shifting that make use of tunable oscillators that sweep over the bandwidth , significantly improving phase shifter bandwidth performance [11]. This improvement not withstanding, a prerequisite for reliable phase scanning is a fine phase resolution that increases hardware complexity. The challenges described above maybe remedied by the use of digital beamformers [11], however, they too require a large number of ADCs that consume a great amount of power. [12] looked at reduction of the number of used ADCs by taking advantage of inter channel correlation, this could only be implemented on analogue beamformers, which as we already mentioned, are limited by phase shifter performance. [13] on the other hand sought to minimize filtering requirements at RF by employing some mixed domain approach for phase shifting and beam-forming in both analogue and digital domains, this approach equally experienced hardware complexity challenge.

In the context of directional selectivity, another approach that has been gaining research track is the Directional Modulation (DM) technique [14] which is specifically concerned with data security at the physical layer. DM attains directionality by intentionally transmitting distorted signals towards all spatial locations apart from the predefined secure spatial communication direction(s). It does well in limiting ability to decode data at the side-lobes but the main lobe selectivity remains the same as for the case for classical beamforming.

Recently, we proposed a novel technique envisaged as an alternative to classical beamforming, Spatial Data Focusing [1–3]. Specifically in [3], SDF employing spread spectrum modulation using orthogonal gold codes was proposed. SDF promises to tackle the twin challenge of minimizing the required hardware and simultaneously increasing locational selectivity. It employs techniques that maps the symbols to be transmitted onto an N-dimensional signal space which are then spread using the orthogonal gold codes that also act as the signal's orthogonal basis, the spread signals are subsequently transmitted over separate paths as uncorrelated signals. Despreading at the receiver is performed using the same time synchronized codes as those used at the transmitter. DSSS-SDF significantly reduces the number of antenna elements required to broadcast data over narrow beam-width, in comparison to classical beamforming scheme. Indeed in this case the beamwidth is defied as the region within which data can be decoded and not the classical half power beamwidth.

In this paper, an overview of classical digital beamforming technique is presented in section 2. Section 3 outlines the proposed DSSS-SDF architecture, demonstrating its capability to realise reduced hardware and increased selectivity. Section 4 will review the channel models and metrics used. Section 5 will cover the simulation ans results and finally the conclusion and perspectives will be developed in section 6.
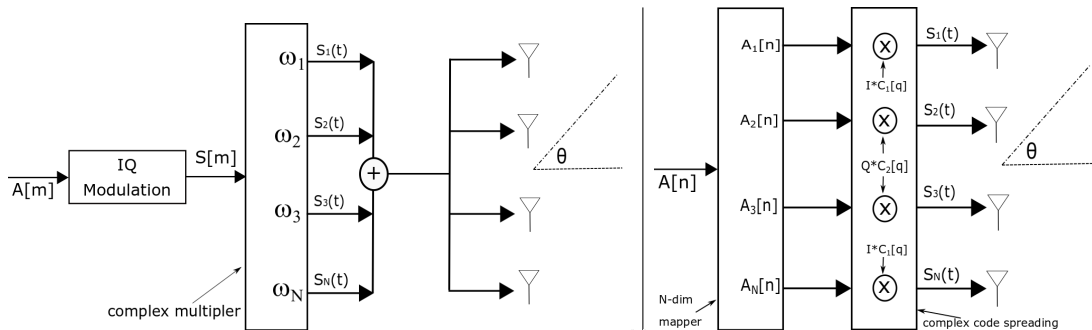

Figure 1 − Transmit architecture of classical beamforming (left) and proposed Orthogonal code based Spatial Data Focusing (right)

2   Digital beamforming

With the coming to age of FPGAs and software defined radio (SDR) in general, communications engineers have prioritised digital beamforming over analogue given the design flexibility that if presents [15]. Specifically, in digital beamforming the RF front end only does the signal reception. The phase shifting and amplitude scaling and combining are all passed to the digital back end as shown in left diagram of figure 1. It is shown that to carry out beamforming the basebnd signals $s[m]$ is multiplied by complex weights ω_i at each of the paths. The complex weight at the ith path is given as $\omega_i = a_i exp^{\phi_i}$, where a_i and ϕ_i are the amplitude and phase weights respectively. Due to beamforming, the signals from the various paths are combined as $S_{out} = \sum_N s[m]\omega_i$. S_{out} is attained by two specific approaches, side lobe control or beam scanning [16].

2.0.1   Side Lobe Control

Side lobes are undesired and lead to reception or transmission of energy in unwanted directions. With beam-forming they can be controlled using amplitude tapering also referred as amplitude weighting. This process varies the excitation amplitude of individual elements in the array. For the case of non-uniformly excited array,

the amplitude taper runs from the array centre to its end to control the minor lobes. Smooth tapers attains larger small side lobe levels but at half-power beam-width. In short, using amplitude tapering on the linear array, it is possible to control the side lobes and achieve a better main beam in the desired direction.

2.0.2 Beam Scanning

Beam scanning is the movement of a radiation pattern in space. It is achieved by controlling the progressive phase difference between the elements to direct the beam in any desired direction [16]. The phase shift changes the phase of the excitation currents of each element in an array. As earlier outlined, apart from digital beamforming, phase shift can be carried out by the use of phase sifter devices, a time delay, frequency scanning or digital beamforming.

3 Principle of Complex Code Direct Sequence Spread Spectrum Spatial Data Focusing

In section 2 we saw that beam formation in power focusing approached is achieved by either manipulating the phase shift or amplitudes, this section introduces Direct Sequence Spread Spectrum approach to SDF, specifically we will demonstrate that SDF attains beam resolution by exploiting time delay of the signals arriving at the receiver from various paths. It will be demonstrated that unlike in beamforming where separate process carry out beamforming and demodulation, in orthogonal code based SDF, the same process responsible for data despreading determines beam resolution. This approach enables this scheme to attain finer beam resolutions at the symbol level and simultaneously minimizing the required hardware. Figure 2 shows plotted results comparing BER and θ results for beamforming and SDF as was seen in [3]. It was shown that to attain similar beam-width of $4°$, IQ-DSSS-SDF and beamforming employed 4 and 12 antennas respectively.

3.1 Transmitter

The transmitter architecture for the IQ-DSSS-SDF is shown on the right hand side of figure 1. $A[n]$, the symbols streams to be transmitted, are mapped into an N-dimensional signal space, $A_i[n]$, $i : 1, 2, ..., N$. A set of $N/2$ complex orthogonal Gold codes $C_{ic}[q] = C_i[q] + jC_i[q]$, $i : 1, ..., N/2$ with $C_i[q] \in [-1, 1]$ are subsequently generated. The mapped data streams are uniquely spread using separate quadrature components of the generated IQ codes, the spread data is subsequently used to separately excite the various elements of the antenna array. Code orthogonality enables efficient separation of the codes at the receiver and significantly reduces inter channel interference (ICI). To minimize the bandwidth requirement, the spread signals are shaped using a root raised cosine filter $g(t)$. The antenna array elements output can be expressed as,

$$s_{i=a}^R(t) = \sum_{n=0}^{\infty} A_i[n] \sum_{q=1}^{L_c} C_i^R[q]g(t - nT - qT_c) \tag{1a}$$

$$s_{i=u}^Q(t) = \sum_{n=0}^{\infty} A_i[n] \sum_{q=1}^{L_c} C_{N+1-i}^I[q]g(t - nT - qT_c) \tag{1b}$$

where T_c, T, and q represent the chip duration, symbol duration and chip index respectively, L_c is the length of the applied orthogonal sequences and $\boldsymbol{a}$ and $\boldsymbol{u}$ are $1 : N/2$ and $(N/2 + 1) : N$ respectively. For the spreading and despreading orthogonal Gold codes are preferred as opposed to Walsh codes, due to the fact that they consistently exhibit narrow auto correlation peak with very low side lobes guarding against false registration of the main peak of the autocorrelation function throughout the whole set of codes that form an orthogonal code family. The diagram to the left part of figure 2 depicts typical orthogonal code autocorrelation function performance. In IQ-DSSS-SDF the beam resolution is made finer with an increase in code length. Similarly orthogonal Gold codes exhibit very good cross correlation functions. This two qualities are at the core of the delay based beam resolution employed by SDF. Indeed the same qualities are employed in the capability to accurately control the phase of the channel coding making it possible to achieve a zero cross correlation with respect to the phase between the channels.

3.2 Propagation Channel Considerations

The simulations were carried over a 6-Ray Urban Canyon Multipath channel model with an impulse response $h_i(t)$ due to each dimension given as; $h_i(t) = \sum_l^L \alpha_{il}\delta(t - \tau_{il})e^{-j\omega\tau_{il}}$, where α_{il} is the wave attenuation constant between TX_i and RX. τ_{il} is the propagation delay due to antenna array elements spatial location with respect to RX. L is the number of multipath components. $l = 1$ will be considered as the LOS path for the individual

N paths. the general equation will be given as,

$$h(t, \tau) = \sum_{i}^{N} \sum_{l}^{L} \alpha_{il} \delta(t - \tau_{il}) e^{-j\omega\tau_{il}} \qquad (2)$$

3.3 Receiver

The received signal $r(t) = \sum_{i}^{N} s_i(t) * h_i(t)$, a convolution of the transmitted signal with the channel response that reduces to,

$$r(t) = \sum_{i=1}^{N} \sum_{l}^{L^{MP}} e^{-j\omega\tau_{il}} s_i(t - \tau_{il}) + z(t) \qquad (3)$$

$z(t)$ is AWGN. The channel output feeds into a matched filter matched to the incoming signals. This approach
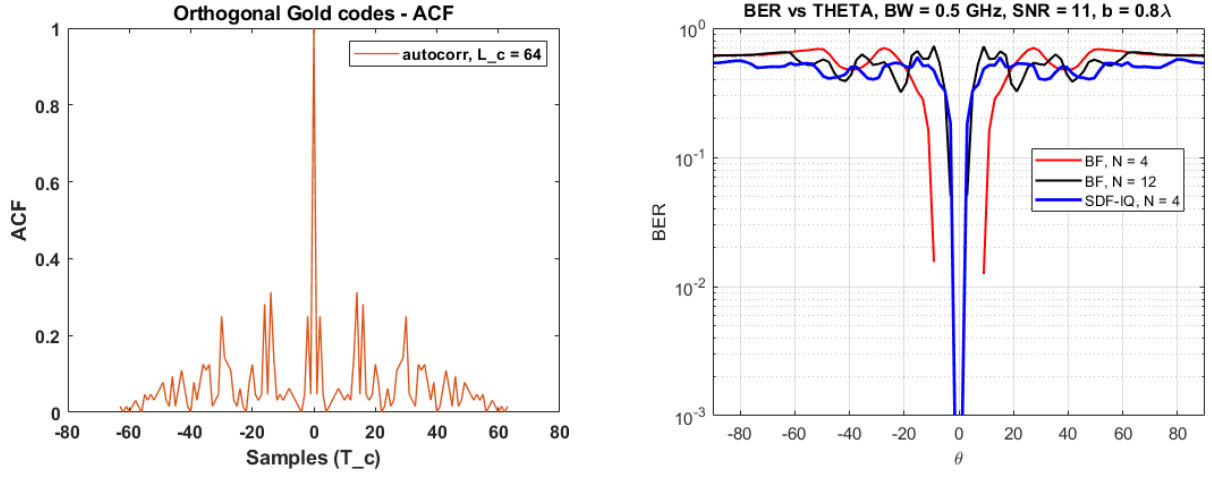

Figure 2 – Typical autocorrelation function for orthogonal Gold codes (left), BER vs θ comparison for BF and SDF applied in LOS scenario(right)

has the advantage of not requiring the use of pilot symbols for synchronization, instead it uses the known code sequences as the reference signal. The output of the matched filter $y(t) = r(t) * g^*(T_c - t)$ is given as:

$$y(t) = \sum_{i=1}^{N} \sum_{l}^{L^{MP}} e^{-j\omega\tau_{il}} s_i(T_c - \tau_{il}) + z(t) \qquad (4)$$

The matched filter output $y(t)$ is passed through an I/Q modulator then sampled periodically every $l_c T_c$. l_c and T_c are the code length and chip duration respectively. The real component of the sampled output is shown in (5).
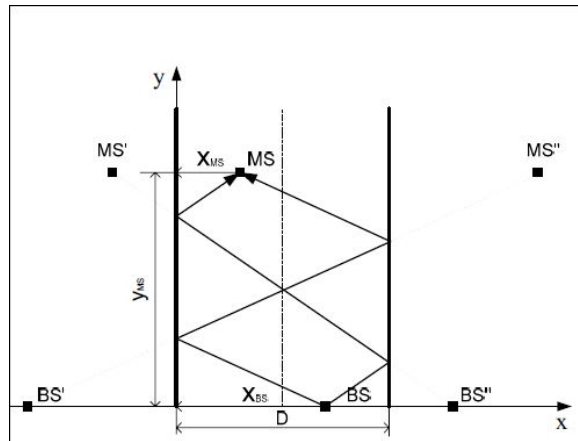

Figure 3 – Geometry of street canyon 6 ray model

$$\hat{y}(l_cT_c) = \sum_{i=0}^{N-1}\sum_{n=0}^{\infty} A_i[n]\Bigg\{\alpha_i^{LOS}\sum_{j=0}^{L_c-1} C^c[j]f(\psi_L)e^{-j\omega\tau_i^{LOS}}$$

$$+ \sum_{l=0}^{L^{MP}-1} R_{il}^{MP}\alpha_{il}^{MP}\sum_{j=0}^{L_c-1} C^c[j]f(\psi_{MP})e^{-j\omega\tau_{il}^{MP}} + z(l_cT_c)\Bigg\} \tag{5}$$

where $\psi_L = ((l_c-j)T_c - nT - \tau_i^{LOS})$ and $\psi_{MP} = ((l_c-j)T_c - nT - \tau_{il}^{MP})$. τ_i^{LOS}, τ_{il}^{MP} and L^{MP} are the propagation delay due to the LOS, NLOS paths and the number of multipath components (MPC) respectively. N is the number of applied dimensions and R_{il}^{MP} is the reflection coefficient due to each MPC [17]. The τ_i^{LOS}, τ_{il}^{MP} are obtained from the various path distances on division by speed of c (speed of light). The distance can be calculated as [17],

$$d(BS,MS)_{LOS} = \sqrt{(X_{MS}-X_{BS})^2 + (Y_{MS}+Y_{BS})^2 + (Z_{MS}-Z_{BS})^2} \tag{6a}$$

$$d(BS,MS)_{GR} = \sqrt{(X_{MS}-X_{BS})^2 + (Y_{MS}+Y_{BS})^2 + (Z'_{MS}-Z_{BS})^2} \tag{6b}$$

$$d(BS,MS)_{LR} = \sqrt{(X'_{MS}-X_{BS})^2 + (Y_{MS}+Y_{BS})^2 + (Z_{MS}-Z_{BS})^2} \tag{6c}$$

$$d(BS,MS)_{RR} = \sqrt{(X''_{MS}-X_{BS})^2 + (Y_{MS}+Y_{BS})^2 + (Z_{MS}-Z_{BS})^2} \tag{6d}$$

$$d(BS,MS)_{RLD} = \sqrt{(X'_{MS}-X''_{BS})^2 + (Y_{MS}+Y_{BS})^2 + (Z_{MS}-Z_{BS})^2} \tag{6e}$$

$$d(BS,MS)_{LRD} = \sqrt{(X''_{MS}-X'_{BS})^2 + (Y_{MS}+Y_{BS})^2 + (Z_{MS}-Z_{BS})^2} \tag{6f}$$

The real and imaginary components coming out of the IQ demodulator are used to acquire the initial synchronisation values. This is done with respect to a reference path with the aid of the known despreading codes generated at the receiver. The results of synchronisation due to the preferred reference path forms the basis for aligning all the members of the despread code sequence as to synchronize them with the incoming signals prior to despreading. The *mth* estimated symbol coefficients derived by cross correlating $\hat{y}_i(l_cT_c)$ with the receiver generated and synchronized codes are given as:

$$\hat{s}_i[m] = \hat{y}(l_cT_c)\sum_{z=mLc+1}^{m+1}\left\{C_{is}^c[z-mLc] + \sum_{i\neq i}^{N} C_{is}^c[z-mLc] + C_{is}^c[z-mLc]z(l_cT_c)\right\} \tag{7}$$

3.4 Beam resolution

As was mentioned earlier, beamwidth in SDF is defined as the area within which data can be decoded. Thus, (7) is responsible for this process. It has three distinct components viz: the desired signal due to autocorrelation function; the cross correlation function; and the noise component. Assuming an ideal scenario, i.e., perfect synchronisation and receiver located at broadside, phase shift with respect to the reference dimension and position is zero. Based on Orthogonal Gold code properties, the cross correlation components will all go to zero, the noise component will be spread out giving low noise energy and the autocorrelation will attain very high peaks thus we can decode the transmitted signal. On the other hand as the receiver moves away from the designated position, the autocorrelation function is no longer at peak, in addition the cross correlation function now introduces interference to the overall signal akin to inter channel interference. Indeed time delay (phase) mismatch with respect to the reference dimension as a function of receiver position will lead to mismatch of the incoming signals with the synchronised copies thus reducing receiver SINR. The likeness of the signal time spaced copies rapidly diminishes with the delay mismatch, this is attributed to the receiver moving away from the targeted geographical location. In summary unlike in classical beamforming where sidelobe control is carried out by amplitude tapering, in IQ-DSSS-SDF, side lobe control is a by product of the correlation process.

3.5 Multipath mitigation

Recall from (5) that $\psi_L = ((l_c-j)T_c - nT - \tau^{LOS})$ and $\psi_{MP} = ((l_c-j)T_c - nT - \tau_{il}^{MP})$. With the assumption of perfect synchronisation and receiver at broadside, $\tau_i^{LOS} = 0$ with respect to LOS path and the synchronised despreading code, this subsequently implies that all delay due to τ_{il}^{MP} will be attenuated by the autocorrelation of the spreading code at time τ_{il}^{MP}.

4 Channel Model Evaluation Metrics

Figure 3 depicts the modelled channel, a classical 5G deployment scenario of the urban micro (UMi) with outdoor to outdoor (O2O) propagation [4]. The power, delay, time, spatial or angular characteristics of the

channel were characterized as shown in figure 4, this outlook at the dispersion of the received signal gave us an understanding of the impact of multipath propagation on IQ-DSSS-SDF.

4.0.1 Power Delay Profile(PDP)

PDP defines the variation of individual path powers with respect to the delay due to the position of the receiver from the transmitter. Ray tracing being a typical deterministic channel model, power and delays are the direct outputs of this channel model.

4.0.2 RMS Delay Spread

The multiple rays introduced by multipath propagation have varying gains and delays. The knowledge of delay spread get us to understand the impact of ISI on the channel. RMS delay spread is required to characterize wide band channels [18]. [19] outlines the approach towards calculation of the standard deviation and mean of the delay spread. The delay spread is given as,

$$DS = \sqrt{\frac{\sum_1^N P_l \tau_l^2}{\sum_1^N P_l} - \tau_0^2} \; ; \quad \tau_0 = \frac{\sum_1^N P_l \tau_l^2}{\sum_1^N P_l} \tag{8}$$

where P_l and τ_l refer the power and the delay of the lth path

4.0.3 RMS angle spread

The dispersion of the received signal in the angular domain is demonstrated using angular spread such that channels exhibiting wide angular spread depict large capacity and those with narrow angular spread on the other depict efficient beamformer design [20]. Angular spread can be derived from two approaches; the first one takes the LOS path as reference and calculates the spreads while the other employs circular wrapping [21]
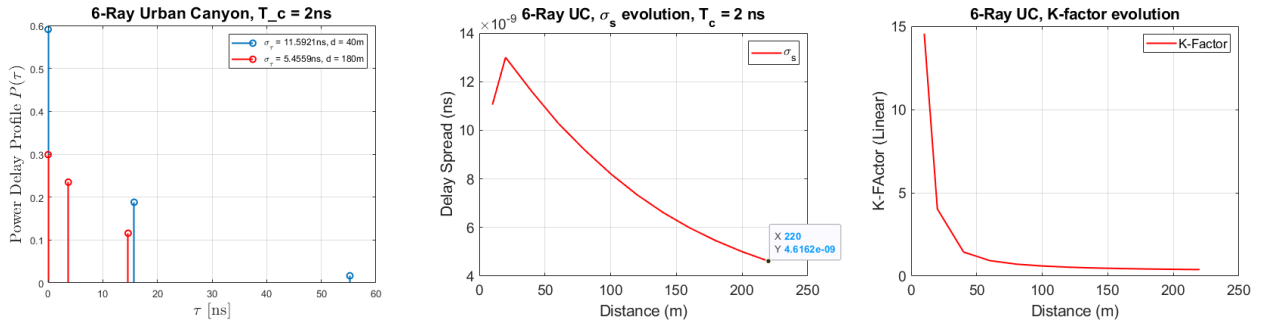

Figure 4 − Channel characterization plots; Power Delay Profile(PDP) (left); Evolution of Delay Spread with distance (centre) and Evolution of K-Factor with distance (right)
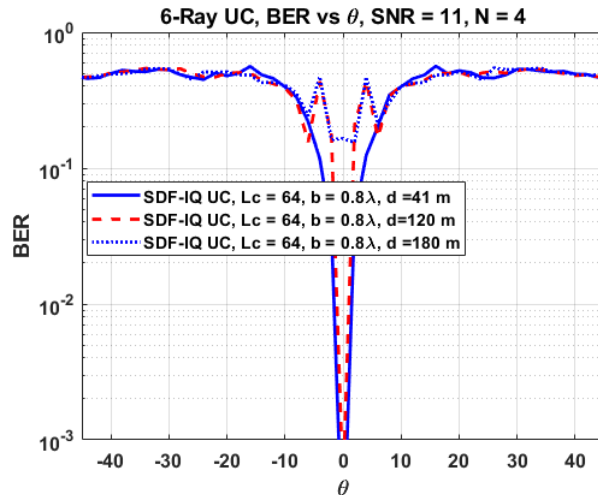

Figure 5 − 6-Ray Urban Canyon, BER vs θ plots

4.0.4 K-factor

The K-factor measures of ratio of the power between the LOS ray and the NLOS ray. In [22] it was shown that an increase in the use of higher bands and access point density leads to an increase in LOS condition thus the K-factor influences the fading statistics of BER, spectral efficiency and mean fading duration. K-factor can be calculated as,

$$KF = \frac{P_{LOS}}{\sum_{l \neq LOS} P'_l} \tag{9}$$

where P_{LOS} is the power from the LOS ray and l is the number of rays.

5 Simulation and Results

This sections outlines the simulation process and the discusses the acquired results. The simulations were carried on Matlab Software. For this specific work orthogonal Gold codes of code length 64 were used. The SNR was set to $11dB$ and occupied bandwidth set at $500MHz$. For channel characterization various distances in metres between the receiver and antenna array were considered (10 - 220 m). The number of elements in the array was set to $N = 4$. Distance between the array elements set to 0.8λ and indeed the chosen channel model is a 6-Ray urban canyon micro-cell.

The first plot of figure 4 depicts power delay profile taken from two ends of the distance. We see that at around 40 metres, i.e, closer to the antenna array, the LOS signal is clearly dominant and the time delay between and the first NLOS is significant a typical Rician channel scenario. On the other hand further away the LOS channel is no more dominant ant the system moves towards a typical Rayleigh scenario. The plot in the centre 4 represents the evolution of the delay spread. Despite the fact that it diminishes with increasing distance, it does not get to non resolvable levels ($T_c > \sigma_s/2$), thus in this case the evolution of delay spread does not impact the system. The third plot to the right depicts the evolution of K-Factor with distance. We see that initially it is high and with distance it reduces to very low level. The lower K-Factor are an indicator that the NLOS signals have power almost equal to or even equal to the LOS signal. In such a scenario K-factor is said to influence the fading statistics of BER, spectral efficiency, and average fading duration.

The above cases come out clearly in the BER vs θ plot of figure 5, where we see that at 41 metres and 120 metres respectively, IQ-DSSS-SDF attained beamwidths of less than $2.3°$ at a set BER threshold of 10^{-3}, on the other hand at around $180m$ the BER was quite high which can be attributed fading as earlier demonstrated reducing K-factor.

6 Conclusion

In this work we have outlined the difference between classical beamforming and DSSS-SDF, as regards the process of beam formation and explained that in beamforming, beam formation is due to amplitude tapering whereas in DSSS-SDF it is a function of time delay that is inherent in the process of correlation. We showed that from earlier work done [3], for a similar size beamwidth, DSSS-SDF and beamforming employed 4 and 12 antennas respectively. We also carried out the characterization of a 6-Ray urban canyon channel and showed how it impacts the signals transmitted vis the DSSS-SDF application

7 References

[1] J. Sarrazin, M. Odhiambo, S. Golstein, P. De Doncker, and F. Horlin, "Spatial data focusing: An alternative to beamforming for geocasting scenarios," in *2018 USNC-URSI Radio Science Meeting (Joint with AP-S Symposium)*, pp. 139–140, July 2018.

[2] Molineaux, G., Golstein, S., Odhiambo, M., Horlin, F., De Doncker, P., & Sarrazin, J. S. J., "Spatial data focusing using time and iq resources for wireless geocasting," in *Proc. of the IEEE Global Communications Conference, GLOBECOM (09-13 December, 2019: Waikoloa, HI, USA)*, Dec 2019.

[3] Odhiambo, M., Golstein, S., Sarrazin, J. S. J., De Doncker, P., & Horlin, F., "Spatial data focusing, implementation using spread spectrum modulation techniques," in *Actes des 21èmes Journées Nationales Micro-ondes, JNM (15-17 May, 2019: Caen, France)*, May 2019.

[4] 38.901 (2018), *Study on channel model for frequencies from 0.5 to 100 GHz. Technical Specification (TS) Release 15, 3rd Generation Partnership Project (3GPP)*. IEEE personal communications, vol. 5, no. 1, pp. 10–22, 2018.

[5] R. Ertel, P. Caroieri, K. Sowerby, T. Rappaport, and J. Reed, *Overview of spatial channel models for antenna array communication systems*, pp. 20–32. United States: John Wiley and Sons Inc., 1 2009.

[6] L. C. Godara, "Application of antenna arrays to mobile communications. ii. beam-forming and direction-of-arrival considerations," *Proceedings of the IEEE*, vol. 85, pp. 1195–1245, Aug 1997.

[7] H. Steyskal, "Digital beamforming antennas - An introduction," *Microwave Journal*, vol. 30, p. 107, Jan 1987.

[8] Volakis J. L, *Antenna engineering handbook. 4th ed. Chapter 3,20,21.* NewYork (NY):McGraw Hill, 2007.

[9] D. Parker and D. C. Zimmermann, "Phased arrays - part 1: theory and architectures," *IEEE Transactions on Microwave Theory and Techniques*, vol. 50, pp. 678–687, March 2002.

[10] J. Blass, "Multidirectional antenna—a new approach to stacked beams," *IRE International Convention Record. New York (NY)*, vol. 8, pp. 48–50, Mar 1960.

[11] H. Hashemi, X. Guan, A. Komijani, and A. Hajimiri, "A 24-ghz sige phased-array receiver-lo phase-shifting approach," *Microwave Theory and Techniques, IEEE Transactions on*, vol. 53, pp. 614 – 626, 03 2005.

[12] J. H. C. van den Heuvel, J. M. G. Linnartz, P. G. M. Baltus, and D. Cabric, "Full mimo spatial filtering approach for dynamic range reduction in wideband cognitive radios," *IEEE Transactions on Circuits and Systems I: Regular Papers*, vol. 59, pp. 2761–2773, Nov 2012.

[13] C. Wijenayake, Y. Xu, A. Madanayake, L. Belostotski, and L. T. Bruton, "Rf analog beamforming fan filters using cmos all-pass time delay approximations," *IEEE Transactions on Circuits and Systems I: Regular Papers*, vol. 59, pp. 1061–1073, May 2012.

[14] T. Hong, M. Song, and Y. Liu, "Dual-beam directional modulation technique for physical-layer secure communication," *IEEE Antennas and Wireless Propagation Letters*, vol. 10, pp. 1417–1420, 2011.

[15] J. Razavilar, F. Rashid-Farrokhi, and K. J. R. Liu, "Software radio architecture with smart antennas: a tutorial on algorithms and complexity," *IEEE Journal on Selected Areas in Communications*, vol. 17, pp. 662–676, April 1999.

[16] Stutzman, W.L. Thiele, *Antenna Theory and Design, 3rd Edition.* New York: Wiley, 2013.

[17] D. Bojanjac, R. Nađ, and G. Šišul, "Ray tracing model of pedestrian urban zone," in *Proceedings ELMAR-2010*, pp. 289–292, Sep. 2010.

[18] M. P. Fitton, A. R. Nix, and M. A. Beach, "A comparison of rms delay spread and coherence bandwidth for characterisation of wideband channels," in *IEE Colloquium on Propagation Aspects of Future Mobile Systems (Digest No: 1996/220)*, pp. 9/1–9/6, Oct 1996.

[19] Saunders S. and Aragón-Zavala A, *Antennas and propagation for wireless communication systems.* John Wiley and Sons, 2007.

[20] Meinilä J., Kyösti P. et al., *Winner+ final channel models v1. 0.* IEEE personal communications, vol. 5, no. 1, pp. 10–22, Jun 2010.

[21] 3GPP, *Circular angle spread. Teleconference, 3rd Generation Partnership Project (3GPP).* 3GPP Project, 2003.

[22] S. Mukherjee, S. S. Das, A. Chatterjee, and S. Chatterjee, "Analytical calculation of rician k-factor for indoor wireless channel models," *IEEE Access*, vol. 5, pp. 19194–19212, 2017.